

Revealing the Geometrical and Vibrational Properties of the Defects Driving the Boson Peak

Shivam Mahajan¹, Darryl Seow Yang Han¹, Cunyuan Jiang^{2,3,4}, Matteo Baggioli^{2,3,*}, and Massimo Pica Ciamarra^{1,*}

¹Division of Physics and Applied Physics, School of Physical and Mathematical Sciences, Nanyang Technological University, Singapore

²Wilczek Quantum Center, Shanghai Jiao Tong University, Shanghai 200240, China

³Shanghai Research Center for Quantum Sciences, Shanghai 201315, China

⁴Department of Fundamental Engineering, Institute of Industrial Science, The University of Tokyo, 4-6-1 Komaba, Meguro-ku, Tokyo 153-8505, Japan

*Corresponding authors: b.matteo@sjtu.edu.cn, massimo@ntu.edu.sg

ABSTRACT

The vibrational density of states is key to understanding the mechanical, thermal, and transport properties of materials. In amorphous solids, this density shows an excess of vibrational modes compared to the Debye model, known as the boson peak, whose origin remains poorly understood. Previous studies have suggested a link between the boson peak and quasi-localized nonphononic vibrations, or "defects." However, it has been difficult to clearly identify these defects, possibly because they hybridize with extended phonons, casting doubt on their existence and connection to the boson peak. In this work, we introduce a simple and practical method for separating hybridized phonons from localized vibrations. We show that phonons at the boson peak frequency hybridize with localized defects. These defects are anisotropic, compact, and exhibit oscillatory pure shear deformations. Their density correlates with the excess of vibrational modes at the boson peak frequency across various two- and three-dimensional systems, confirming that they are the microscopic origin of the boson peak.

Thermal and vibrational properties of amorphous solids display universal characteristics that are very different from their crystalline counterparts [1]. In particular, their vibrational density of states (vDOS) $D(\omega)$ presents a universal excess anomaly over the Debye prediction $D(\omega) \propto \omega^{D-1}$, with D the number of spatial dimensions and ω the frequency, known as the "boson peak" (BP). The microscopic origin of the BP remains one of the most controversial topics in condensed matter physics.

Some theories assume that BP arises from additional nonphononic excitations associated with quasi-localised modes (QLMs). The observation that structural glasses present nonphononic excitations is old [2]. This idea was inspired (see *e.g.* [3]) by the concept of resonant modes first formulated in the context of defective crystals [4] and it is a recurrent theme within the soft potential model of glassy anomalies [5–8]. These nonphononic excitations have been widely reported in the low-frequency spectrum of amorphous solids and even disordered crystals [9], where they contribute to the density of states with a faster than Debye term, $D(\omega) \propto \omega^p$ with $p > (D - 1)$, [10–12]. They have a quadrupolar nature and are characterized by a core made of few atoms accompanied by long-range displacements with power-law decay [13]. It has been argued that QLMs also exist at the boson peak frequency and cause the boson peak [7, 8, 14–17]. However, this scenario is difficult to prove, as QLMs would strongly hybridize with extended phononic modes around the BP frequency, rendering their identification [6, 18] and the study of their properties problematic. Henceforth, the existence of localised modes at the boson peak is questionable, motivating the development of alternative theories of the BP [19–25].

Recent works have explored the possibility of disentangling QLMs and extended modes at the boson peak frequency. In one approach, deformations with seemingly quadrupolar structures were studied within the vibrational modes at the boson peak frequency to assess whether they could serve as seeds for energy-minimal localized deformations [16, 17], which are identified with QLMs. Alternatively, Refs. [25, 26] examined how modes near the boson peak contribute to the amplitude of particle vibrational motion (see also [3]). Particles receiving significant contributions from these modes tend to form clusters, possibly emerging as a consequence of the hybridization of phonons and QLMs, and referred to as stringlets [25, 26] due to their resemblance to one-dimensional string-like or ring-like dynamical defects. Furthermore, the interaction between stringlets and phonons induces a flat boson peak mode [27, 28], observed in both simulations [25] and experiments [29]. This supports the hypothesis that stringlets, rather than quasi-localized quadrupolar modes, may be the microscopic origin of the boson peak, even in heated crystals [30]. It remains unclear whether localized defects are responsible for the boson peak in glasses and

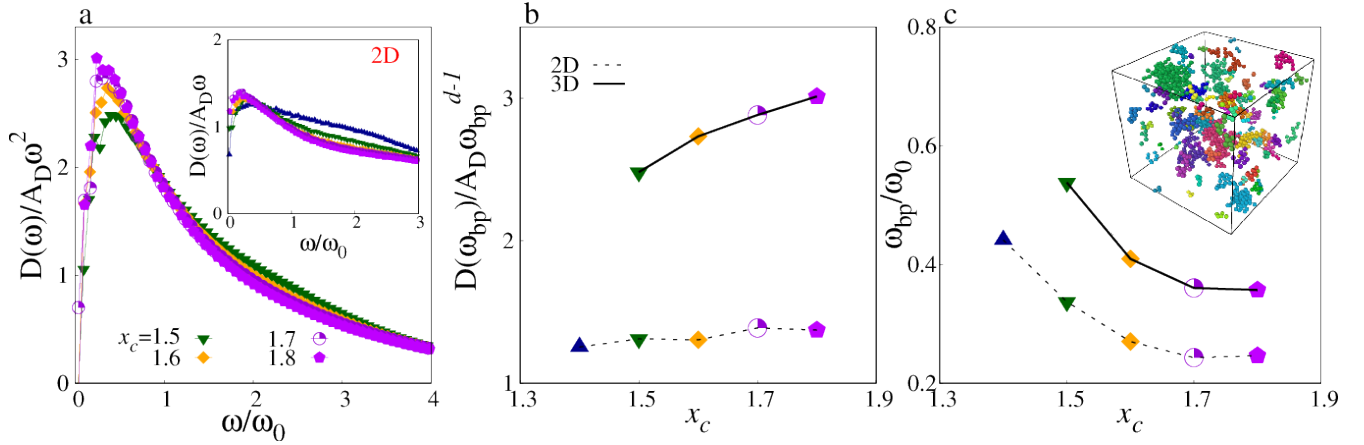


Figure 1. Attraction regulates the boson peak in 2D and 3D amorphous solids. **a** The reduced vDOS in three and (inset) two dimensions for systems differing in the extension x_c of the intermolecular attractive potential well. In 3D, the materials lose stability as x_c increases, as the boson peak intensity increases **(b)** while its frequency decreases **(c)**. In 2D, attraction does not sensibly influence the excess vibrational modes. Frequencies are expressed in units of the natural frequency $\omega_0 = c_s/a_0$, with a_0 the interparticle spacing and c_s the shear wave speed. The inset of **(c)** illustrates the localised defects that, according to our investigation, induce the boson peak in a three-dimensional system with $x_c = 1.7$.

whether these defects are quasi-localized quadrupolar modes or string-like excitations, leaving the microscopic origin of the boson peak unresolved.

In this work, we resolve this tension by introducing a simple and efficient method based on cage-relative displacement to disentangle extended phonons from quasi-localized defects. We demonstrate that the modes at the boson peak frequency are a superposition of phonons and anisotropic, compact localized defects, exhibiting pure shear oscillatory deformations in two and three spatial dimensions. We show that the density of these defects explains the excess number of modes at the boson peak, providing strong support for previous suggestions that the boson peak originates from quadrupolar quasi-localized excitations [15, 16]. Additionally, we identify the so-called stringlets [25], revealing that, contrary to earlier speculations, they are not string-like objects but compact ones that align with the localized defects we have uncovered. Our work unifies different theoretical perspectives on the boson peak in glasses, resolving the long-standing debate and potentially establishing a consensus on its microscopic origin.

Models and vibrational density of states

We numerically investigate the vibrational properties of two- and three-dimensional systems of polydisperse particles interacting via a Lennard-Jones-like potential $U(r_{ij}, x_c)$ which vanishes with its first two derivatives at $x_c\sigma$, σ being the average particle diameter [31, 32]. We provide details in [Methods](#). Previous works have shown that x_c , which controls the extension of the attractive well, influences the system's relaxation dynamics [32] and the mechanical response [31, 33–35]. We simulate $N = 256k$ particle systems in square or cubic simulation boxes with periodic boundary conditions at fixed interparticle spacing $a_0 = \rho^{-1/d} \simeq 0.977$. We generate amorphous solid configurations by minimizing, via conjugate gradient, the energy of systems in thermal equilibrium in the NVT ensemble at $T = 4.0\epsilon$, above the glass transition temperature for the considered x_c values [32]. All data presented below are averaged over 200 configurations at each x_c .

We evaluate the vibrational density of states (vDOS) over a broad frequency range by performing a Fourier transform of the velocity autocorrelation function in the linear response regime. Additionally, we compute the vDOS by directly diagonalizing the Hessian matrix, allowing us to access the eigenvectors, \mathbf{e}_k , and eigenfrequencies, ω_k , in a low-frequency regime that includes the boson peak (BP) frequency. The two methods give consistent results (see [SI](#)). Fig. 1(a) illustrates the reduced-vDOS $D(\omega)/A_D\omega^D$, with $D_{\text{Debye}} = A_D\omega^D$ Debye's prediction (see [SI](#)), and demonstrates the BP in both two and three spatial dimensions. In 3D, the normalized peak amplitude increases with x_c while its frequency ω_{bp} decreases, indicating that shorter attractive wells lead to more stable glasses, as previously suggested [15, 31, 33, 35]. Due to the increase in stability limit we consider $x_c \geq 1.4\sigma$; at smaller x_c , phonons band structure persists to high frequency given our considered system sizes, making ω_{bp} of difficult identification. In 2D, the role of x_c is minor. In this case, we consider $x_c \geq 1.4\sigma$; at smaller x_c the BP peak becomes very broad and ω_{bp} of difficult estimation.

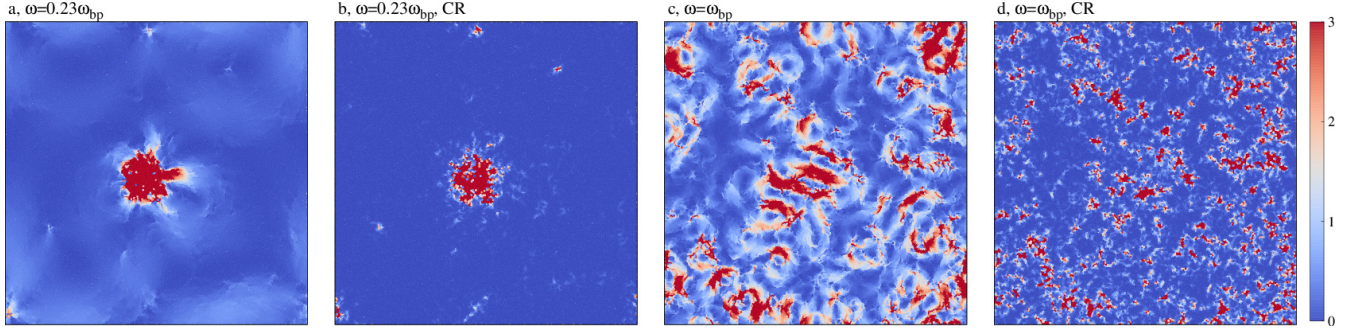


Figure 2. Disentangling extended plane waves and localised defects. **a** Colour map of the magnitude $|\mathbf{e}_{k,i}|^2$ of the particle displacement associated with a low-frequency mode with $\omega_k = 0.23\omega_{\text{bp}}$. A localized defect is visible. **b** The defect remains visible in the colour map of the magnitude of the cage-relative (CR) displacement, $|\mathbf{e}_{k,i}^{\text{cr}}|^2$. Panels **c** and **d** use the same approach to visualize the mode at the BP frequency. In this case, the cage-relative measure reveals the presence of many vibrational defects not apparent in the standard measure. In all plots, the magnitudes are scaled so that their average value is 1.

Disentangling phonons and localised defects

Due to the interaction with phonons, localised vibrations cannot be directly visualized as harmonic vibrations when their frequency is inside a phonon band. Instead, the phonons-defect hybridization leads to extended harmonic modes combining the two. Devising strategies to disentangle this hybridization and expose the localised defects is a longstanding challenge. Two approaches have been introduced so far: one relies on the assumption that the localised defects appear in regions where the local vibrational kinetic energy is high [3, 25, 26], and the other on the hypothesis that these defects have a quadrupolar structure visible in the hybridized field [16, 17].

We propose an alternative, simple and practical approach to disentangle localised defects and extended plane waves based on the hypothesis that plane waves at the BP frequency are locally affine while localised defects are not. Diverse approaches could be employed to identify regions of local non-affine behaviour [36]. Here we rely on the cage-relative displacement field, which has been previously used to filter out the effect of long-wavelength plane waves [37–39], to separate and remove the plane-wave contribution from the eigenvectors. This approach involves analyzing particles’ displacements relative to their immediate surroundings or the ‘cage’ formed by neighbouring particles. Specifically, given a displacement field \mathbf{u} , the cage-relative displacement \mathbf{u}_i^{cr} of particle i is $\mathbf{u}_i^{\text{cr}} = \mathbf{u}_i - \frac{1}{N_v} \sum_{j=1}^{N_v} \mathbf{u}_j$, where the summation extends over the N_v Voronoi neighbors of particle i . We use this approach by considering as displacement fields the vibrational modes of the systems, \mathbf{e}_k , which we determine via the direct diagonalization of the Hessian matrix. We consider as defective particles those with an $|\mathbf{e}_{k,i}^{\text{cr}}|^2$ value in the top 5%, unless otherwise specified, and determine the vibrational defects via a cluster analysis of these particles, considering two particles as belonging to the same cluster if Voronoi neighbors.

We validate our approach in Fig. 2. First, we demonstrate that this method does not filter out localized vibrations. In panel (a), we present a snapshot of a two-dimensional system where each particle is colour-coded based on its $|\mathbf{e}_{k,i}|^2$, for a low-frequency localised mode k . The localised excitation remains clearly visible in panel (b), where particles are coloured according to the magnitude of their cage-relative displacement, $|\mathbf{e}_{k,i}^{\text{cr}}|^2$, proving that our approach preserves localized defects. In panels (c) and (d), we compare the magnitude of the displacement and cage-relative displacement for the mode at the boson peak frequency. The cage-relative measure effectively filters out the collective translations responsible for the extended clusters in panel (c), revealing defective regions of large non-affine particle motion. This approach works equally well in three-dimensional systems, as shown in the inset of Fig. 1(c). Additional evidence in the Supplementary Information (SI) shows that cage-relative measures successfully filter out plane wave contributions at the boson peak frequency.

Geometrical properties of vibrational defects

Fig. 3(a) shows that the probability distribution of the number of particles in a cluster $P(n)$ decays abruptly at small n and roughly exponentially at larger n , similar to the distribution of the number of particles participating in the stringlets [25, 40, 41]. On increasing x_c , the average cluster size varies from $\langle n \rangle = 16$ to 26, in 3D, and $\langle n \rangle = 9$ to 13, in 2D. The average coordination number $z(n)$ grows with n due to the competition between bulk and surface particles, as in Fig. 3(b), and it is larger than two if not for minute clusters, indicating that the clusters are not string-like. To assess a cluster’s geometrical properties, we perform a principal component analysis of the covariance matrix $C_{\alpha\beta} = \langle r_\alpha r_\beta \rangle - \langle r_\alpha \rangle \langle r_\beta \rangle$ of the positions of its particles. We use the eigenvalues λ_i of $C_{\alpha\beta}$, which measure the variances of the particle positions along the principal directions, to define normalized standard deviations $\sigma_i = \sqrt{\lambda_i} / \sum_i \sqrt{\lambda_i}$ that obey the geometrical constraint $\sum_i \sigma_i = 1$, and order them such that $\sigma_{i+1} > \sigma_i$. In two dimensions, $\sigma_1 = 1$ for linear (maximally anisotropic, one-dimensional) clusters and $\sigma_1 = \frac{1}{2}$ for circular (isotropic) clusters.

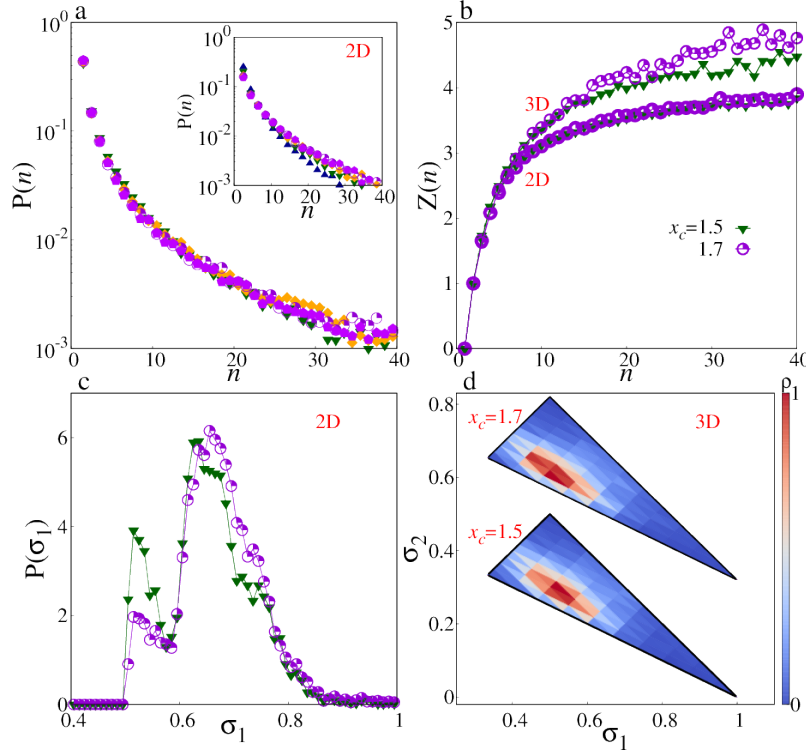


Figure 3. Geometrical properties of vibrational defects. **a** Probability distribution of the number of particles belonging to each defect in 3D and 2D (inset). Symbols identify the values of x_c , as in Fig. 1b. **b** Average coordination number of the particles in clusters of size n . **c** We normalise ($\sum \sigma_i = 1$) and order ($\sigma_i > \sigma_{i+1}$) the standard deviations of the particles' positions along the principal axis of each 'defect', considering defects with at least $n = 3$ particles. In two dimensions, the probability distribution of $P(\sigma_1)$ peaks at intermediate values and drops at large ones, indicating that the defects are not one-dimensional ($\sigma_1 = 1$), but two-dimensional objects, albeit not precisely circular ($\sigma_1 = 1/2$). **d** In three dimensions, the probability distribution $P(\sigma_1, \sigma_2)$ clarifies that clusters are not one-dimensional ($\sigma_1 = 1$) or two-dimensional ($\sigma_1 + \sigma_2 = 1$). We thus assume they are three-dimensional, albeit non-spherical ($\sigma_1 = \sigma_2 = 1/3$). Data for $x_c = 1.7$ are shifted vertically for clarity.

We find that the distribution $P(\sigma_1)$ peaks at $\sigma_1 \simeq 0.65$ and vanishes for $\sigma_1 > 0.8$, as shown in Fig. 3(c). This result further confirms that defects are not one-dimensional but rather asymmetric two-dimensional structures.

In three dimensions, for linear (1D), flat (2D), and spherical (isotropic 3D) clusters, $\sigma_1 = 1$, $\sigma_1 + \sigma_2 = 1$, and $\sigma_1 = \sigma_2 = \sigma_3 = \frac{1}{3}$, respectively. Fig. 3(d) presents density maps of the $P(\sigma_1, \sigma_2)$ probability distribution at $x_c = 1.4$ and $x_c = 1.7$ (shifted vertically) and suggests the localised defects have three-dimensional geometry with a variable degree of anisotropy.

Quadrupolar nature of vibrational defects

We obtain an insight into the vibrational nature of these defects by considering that the cage-relative displacement is conceptually related to a local strain tensor, as they are both insensitive to local uniform translations. We thus evaluate the local strain tensor $\boldsymbol{\varepsilon} = \frac{1}{2}(\nabla \mathbf{e} + (\nabla \mathbf{e})^T)$, associated with the displacement field (eigenvector, \mathbf{e}) of the mode at the boson peak frequency, coarse-grained on grids of side-length $w \simeq 1.1$. We decompose this tensor into its volumetric and deviatoric components: $\boldsymbol{\varepsilon} = \boldsymbol{\varepsilon}_{\text{vol}} + \boldsymbol{\varepsilon}_{\text{dev}}$. $\boldsymbol{\varepsilon}_{\text{vol}}$ represents local volumetric deformations. In contrast, the traceless deviatoric component represents volume-preserving deformations, which dominate the vibrational spectrum at the boson peak [42]. The eigenvalues v_k of $\boldsymbol{\varepsilon}_{\text{dev}}$ satisfy the traceless condition $\sum v_k = 0$ and define a local quadrupolar charge $Q_{\text{loc}} = (\frac{1}{2} \sum_{k=1}^D v_k^2)^{1/2}$ [43, 44].

Fig. 4(a) demonstrates a high Pearson correlation coefficient between the local quadrupolar charge and the coarse-grained cage-relative displacement magnitude, consistently with the expected analogy between local strain and cage-relative measure. Since defects are clusters of particles with significant coarse-grained cage-relative displacement, we calculate the deviatoric strain of a defect by summing the deviatoric strain of the individual particles within it. Specifically, we define a cluster deviatoric strain as $\mathcal{E}_{\text{dev}} = \sum \boldsymbol{\varepsilon}_{\text{dev}}$, where the sum extends over all bins containing particles of the considered cluster. The eigenvectors \mathbf{U}_k and eigenvalues Υ_k of \mathcal{E}_{dev} describe the vibrational motion of the cluster. A cluster extends into the directions with $\Upsilon_k > 0$ while it shrinks in the others for half period of oscillation, with particles reversing their direction of motion during the remaining half

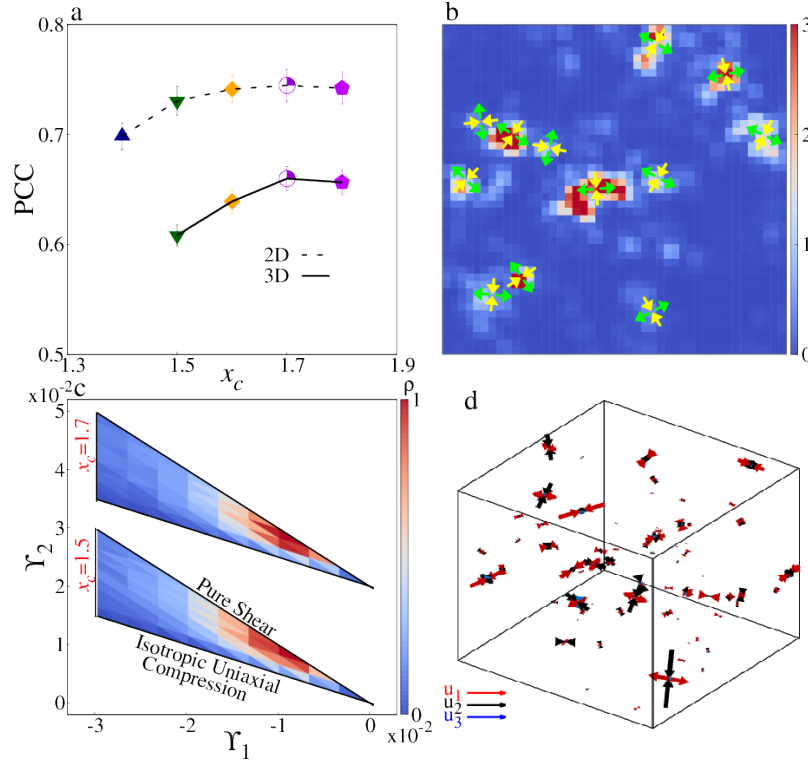


Figure 4. Quadrupolar nature of defects. **a** Pearson correlation coefficient between coarse-grained cage-relative displacement and quadrupolar charge. **b** Quadrupoles associated with the cluster superimposed on a heat map of the magnitude of the coarse-grained cage-relative displacement, normalised by its average value. The figure refers to $x_c = 1.7$ and depicts 1/12th of the system's area. **c** Density map of the two largest (in modulus) eigenvalues of the deviatoric strain associated with the defects, normalised to its maximum value. The density is higher close to the $Y_2 = -Y_1$ line, implying that the quadrupoles correspond to pure shear deformations. **d** We represent the quadrupolar deformations by attaching to each defect's centre of mass the displacements along the principal axis $\pm Y_1 \mathbf{u}_1$ (blue), $\pm Y_2 \mathbf{u}_2$ (green) and $\pm Y_3 \mathbf{u}_3$ (red). Since quadrupoles mostly correspond to pure-shear deformations, \mathbf{u}_3 is barely visible.

period. In the following, we assume $Y_1 < 0$ and order the eigenvalues so that $|Y_i| > |Y_{i+1}|$.

In two dimensions, the traceless condition implies $Y_1 = -Y_2$. Figure 4(b) illustrates the quadrupoles associated with each cluster on a heat map of the magnitude of the coarse-grained cage-relative displacement, finding expected correlations in light of panel (a). The figure illustrates a small fraction of the system and represents each quadrupole with four arrows with a length proportional to $\pm Y_i \mathbf{u}_i$.

In three dimensions, we examine the relevance of various deformation modes that satisfy the traceless condition $\sum Y_i = 0$ by analyzing the probability distribution $P(Y_1, Y_2)$. This distribution is supported within a range defined by the line $Y_1 + Y_2 = 0$, which represents pure shear deformation, and the line $Y_1 + 2Y_2 = 0$, which corresponds to volume-preserving isotropic ($Y_3 = Y_2 = -Y_1/2$) uniaxial compressions. Figure 4(c) shows that quadrupolar deformations are predominantly pure shear, as $P(Y_1, Y_2)$ peaks near the $Y_1 + Y_2 = 0$ line for different values of x_c . This result is further supported by direct visualization of the quadrupoles (Figure 4(d)), depicted as collections of 6 arrows with lengths proportional to $\pm Y_i \mathbf{u}_i$. Since $|Y_3| \ll |Y_2|$, the blue arrows corresponding to displacements in the \mathbf{u}_3 direction are not visible, making the quadrupoles appear as a two-dimensional cross.

The localised defects regulate the boson peak

We test more rigorously whether quadrupolar defects regulate the boson peak by evaluating if their density ρ_d (number per unit volume) accounts for the excess density of vibrational modes defined as $\Delta D(\omega_{bp}) = D(\omega_{bp}) - D_{\text{Debye}}(\omega_{bp})$, where $D_{\text{Debye}}(\omega_{bp}) = A_D \omega^{D-1}$ represents Debye's prediction, as expected if the phonon-defect interaction is weak. In making this test, it is important to note that ρ_d is not uniquely determined, as it depends on the definition of defects used. We define defects as clusters of particles with cage-relative displacements in the top 5%. This threshold is not critical, as the SI shows that varying it does not significantly affect the number of defects or ρ_d , as it primarily impacts the defect size. Instead, the density of defects

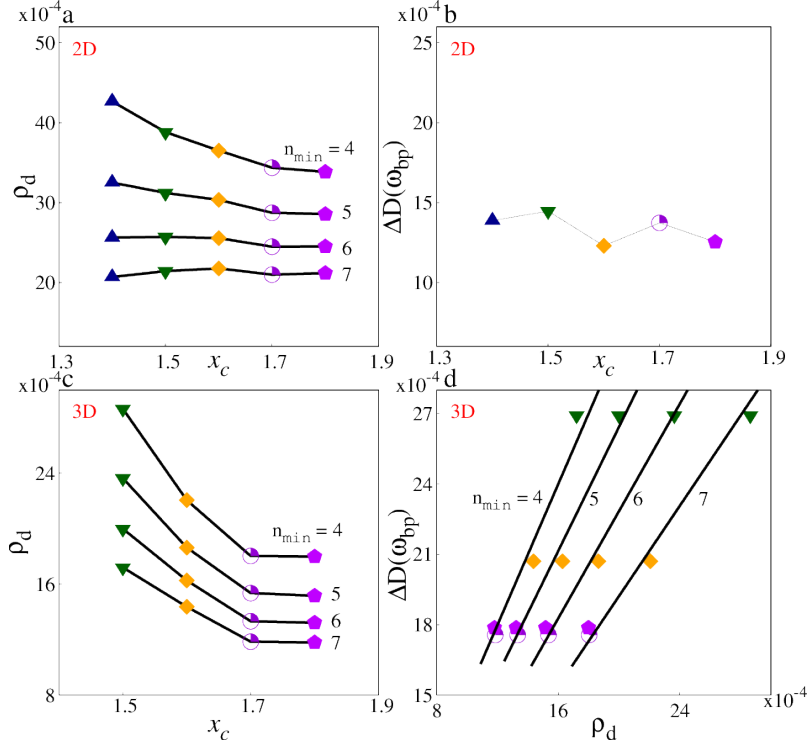


Figure 5. Density of vibrational defects and excess density of modes. We evaluated the excess density of vibrational modes at the boson peak frequency, $\Delta D(\omega_{bp}) = D(\omega_{bp}) - D_{\text{Debye}}(\omega_{bp})$, $D_{\text{Debye}}(\omega)$ being Debye’s density of state, and the density ρ_d of vibrational defects containing more than n particles. In two dimensions, **a** ρ_d for clusters containing a minimum number of particle n_{\min} is x_c independent. Similarly, **b**, $\Delta D(\omega_{bp})$ is x_c independent. In three dimensions, **c** $\Delta D(\omega_{bp})$ grows with x_c , and **d** $\rho_d \propto \Delta D(\omega_{bp})$.

is more influenced by the minimum number of particles, n_{\min} , required for a cluster to be considered a defect. This threshold is introduced to ensure that volume-preserving deformations involve more than just a few particles.

Fig. 5(a) explores the dependence of the density of defects on x_c in two-dimensional systems. An n_{\min} increases, ρ_d quickly loses any x_c dependence. Similarly, we show in panel (b) that the excess of modes $\Delta D(\omega_{bp})$ is also constant in two dimensions, showing therefore a clear correlation with the also constant ρ_d . In three dimensions, Fig. 5(c) demonstrates that the density of defects increases as x_c decreases, consistent with the loss of stability. The excess of modes follows the same trend with x_c , with Fig. 5(d) demonstrating their proportionality. Importantly, in 2D, $\Delta D(\omega_{bp})$ and ρ_d have comparable values, besides being both x_c independent. In 3D, we find that $\Delta D(\omega_{bp}) = c\rho_d$. The constant of proportionality c depends on the specific definition of defects, but it is consistently of order 1. These findings strongly suggest that the excess of vibrational modes at the boson peak frequency originates from the quadrupolar defects we have identified.

Discussion and relation to stringlets

We have identified localised defects hybridizing with plane waves at the boson peak frequency through a filtering technique based on the physical insight that localized vibrations are generally less affine than extended ones. This technique allowed us to isolate the vibrational defects and study their geometrical and vibrational properties. The vibrational defects have some degree of spatial anisotropy but are compact rather than planar or string-like. Their oscillatory motion is quadrupolar. Specifically, the defects undergo pure shear oscillatory deformations, extending along one axis while contracting along a perpendicular one in both two and three spatial dimensions. Analysis of various two- and three-dimensional systems shows that the number density of these defects quantitatively accounts for the excess of modes at the boson peak, confirming their physical relevance.

At this point, one might then wonder how our findings are compatible with the recent claims by Hu and Tanaka [25], that on the contrary identify the microscopic origin of the BP in one-dimensional string-like dynamical objects. These ‘stringlets’ are defined as clusters of particles with a large vibrational amplitude, or equivalently, a high ‘vibrability’ $\Psi_i = \sum_k \frac{1}{\omega_k^2} |\mathbf{e}_{k,i}|^2$, where the sum extends over all modes with frequencies ω_k close to the boson peak frequency $|\omega_{bp} - \omega_k| < \Delta\omega$. We have performed the same stringlet analysis in our simulation model. As shown in Figure 6(a) by the average coordination number of the

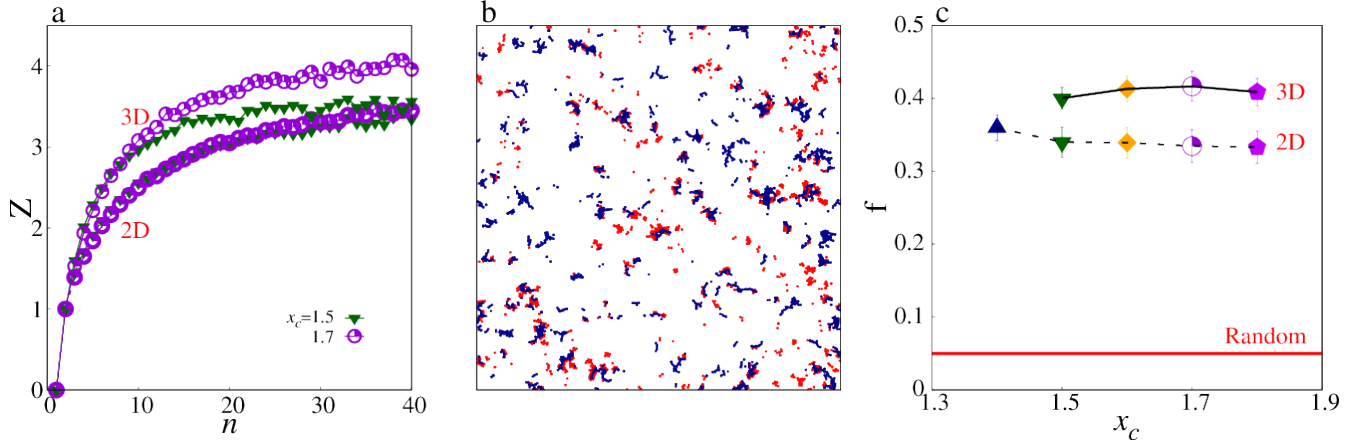


Figure 6. Reconciling stringlets and quadrupolar defects. **a** The coordination number of vibrability clusters increases with n , following a trend similar to that of clusters formed based on cage-relative displacement (Fig. 3c). **b** Particles exhibiting high cage-relative displacement at the boson peak (red) and high vibrability (blue), both in the top 5%, for $x_c = 1.7$. Strong correlations between the two are observed. **c** The fraction of particles displaying both large cage-relative displacement and high vibrability significantly exceeds the expectation under random conditions.

particles participating in the stringlets, we find that the clusters defined as in [25] are compact and extended objects, rather than one-dimensional, very similar to the localised defects found in our work (Figure 3(b)). In Figure 6(b), we observe a high spatial correlation between particles with vibrability in the top 5% (red) alongside those with cage-relative displacements in the top 5% (blue), indicating a high correlation between vibrational motion and cage-relative displacement at the BP frequency. These correlations are further confirmed by measuring the fraction f of particles with high vibrability and cage-relative displacement, which would be $f_{\text{rand}} = 0.05$ in the absence of correlations. Figure 6(c) shows that f is independent of x_c and significantly exceeds the random expectation.

Our analysis provides strong evidence that quadrupolar localised defects and high-vibrability clusters (previously identified as stringlets) are *two sides of the same coin*. This reconciles two of the most successful theories for the origin of the BP in glasses and reveal the ultimate nature of the defects responsible for it.

Along the lines of [15], it would be interesting to understand whether the same defective structures could be also rationalized by means of shear modulus fluctuations and whether our findings are compatible with another successful theory of the BP – heterogeneous elasticity theory [45]. Moreover, it would be fruitful to investigate the relation between the defects discussed in our manuscript and (I) the geometric charges responsible for plastic screening and anomalous elastic response [46], (II) the topological vortex-like defects recently connected to plastic soft spots [47, 48].

Methods

Numerical model

We consider two- and three-dimensional systems of particles of diameter σ_i , drawn from a uniform random distribution in the range $[0.8:1.2]$, that interact via family of LJ-like potentials consisting of a repulsive and an attractive part, $U(r_{ij}, x_c) = U_r(r_{ij}) + U_a(r_{ij}, x_c)$ [31, 32]. The repulsive part follows the standard LJ functional form,

$$U_r(r_{ij}) = 4\epsilon \left[\left(\frac{\sigma_{ij}}{r_{ij}} \right)^{12} - \left(\frac{\sigma_{ij}}{r_{ij}} \right)^6 \right], \quad (1)$$

where $\sigma_{ij} = (\sigma_i + \sigma_j)/2$, but only acts for $r_{ij} \leq r_{ij}^{\min} = 2^{1/6} \sigma_{ij}$. The attractive part, which only acts for distances in the range $2^{1/6} \sigma_{ij} \leq r_{ij} \leq x_c \sigma_{ij}$, is given by

$$U_a(r_{ij}) = \epsilon \left[a_0 \left(\frac{\sigma_{ij}}{r_{ij}} \right)^{12} - a_1 \left(\frac{\sigma_{ij}}{r_{ij}} \right)^6 + \sum_{l=0}^3 c_{2l} \left(\frac{r_{ij}}{\sigma_{ij}} \right)^{2l} \right]. \quad (2)$$

The parameters a_0, a_1 and c_{2l} are chosen such that the potential $U(r_{ij})$ and its first two derivatives are continuous at the minimum r_{ij}^{\min} and at the cutoff $r_{ij}^{(c)} = x_c \sigma_{ij}$, where the potential also vanishes. The parameter x_c sets the extension of the

attractive well [31], which vanishes at $x_c\sigma$. This parameter influences the relaxation dynamics [32] and the mechanical response [31, 33–35].

Data availability

The datasets generated and analysed during the current study are available upon reasonable request by contacting the corresponding authors.

Funding

MPC acknowledges support by the Singapore Ministry of Education through grants MOE-T2EP50221-0016 and RG152/23. CJ and MB acknowledge the support of the Shanghai Municipal Science and Technology Major Project (Grant No.2019SHZDZX01). MB acknowledges the support of the sponsorship from the Yangyang Development Fund.

Author contributions statement

M.P.C. and M.B. devised the project. M.P.C., S.M. and M.B. wrote the paper. S.M., D.S.Y.H. performed the numerical simulations and prepared the figures. All authors contributed to the scientific discussion and refinement of the manuscript.

References

1. Ramos, M. A. *Low-Temperature Thermal and Vibrational Properties of Disordered Solids* (World Scientific (Europe), 2022).
2. Rosenstock, H. B. Anomalous specific heat of disordered solids. *J. Phys. Chem. Solids* **23**, 659–664, DOI: [https://doi.org/10.1016/0022-3697\(62\)90525-5](https://doi.org/10.1016/0022-3697(62)90525-5) (1962).
3. Schober, H. Quasi-localized vibrations and phonon damping in glasses. *J. Non-Crystalline Solids* **357**, 501–505, DOI: <https://doi.org/10.1016/j.jnoncrysol.2010.07.036> (2011).
4. Maradudin, A. A., Montroll, E. W., Weiss, G. H. & Ipatova, I. *Theory of lattice dynamics in the harmonic approximation*, vol. 3 (Academic press New York, 1963).
5. Yu.M. Galperin, V. K. & Kozub, V. Localized states in glasses. *Adv. Phys.* **38**, 669–737, DOI: [10.1080/00018738900101162](https://doi.org/10.1080/00018738900101162) (1989).
6. Schober, H. R. & Oligschleger, C. Low-frequency vibrations in a model glass. *Phys. Rev. B* **53**, 11469–11480, DOI: [10.1103/PhysRevB.53.11469](https://doi.org/10.1103/PhysRevB.53.11469) (1996).
7. Gurevich, V. L., Parshin, D. A. & Schober, H. R. Anharmonicity, vibrational instability, and the boson peak in glasses. *Phys. Rev. B* **67**, 094203, DOI: [10.1103/PhysRevB.67.094203](https://doi.org/10.1103/PhysRevB.67.094203) (2003).
8. Parshin, D. A., Schober, H. R. & Gurevich, V. L. Vibrational instability, two-level systems, and the boson peak in glasses. *Phys. Rev. B* **76**, 064206, DOI: [10.1103/PhysRevB.76.064206](https://doi.org/10.1103/PhysRevB.76.064206) (2007).
9. Lerner, E. & Bouchbinder, E. Disordered crystals reveal soft quasilocalized glassy excitations. *Phys. Rev. Lett.* **129**, 095501, DOI: [10.1103/PhysRevLett.129.095501](https://doi.org/10.1103/PhysRevLett.129.095501) (2022).
10. Lerner, E., Düring, G. & Bouchbinder, E. Statistics and properties of low-frequency vibrational modes in structural glasses. *Phys. Rev. Lett.* **117**, 035501, DOI: [10.1103/PhysRevLett.117.035501](https://doi.org/10.1103/PhysRevLett.117.035501) (2016).
11. Shimada, M., Mizuno, H., Wyart, M. & Ikeda, A. Spatial structure of quasilocalized vibrations in nearly jammed amorphous solids. *Phys. Rev. E* **98**, 060901, DOI: [10.1103/PhysRevE.98.060901](https://doi.org/10.1103/PhysRevE.98.060901) (2018).
12. Wang, L. *et al.* Low-frequency vibrational modes of stable glasses. *Nat. communications* **10**, 26, DOI: [10.1038/s41467-018-07978-1](https://doi.org/10.1038/s41467-018-07978-1) (2019).
13. Lerner, E. & Bouchbinder, E. Low-energy quasilocalized excitations in structural glasses. *The J. Chem. Phys.* **155**, 200901, DOI: [10.1063/5.0069477](https://doi.org/10.1063/5.0069477) (2021).
14. Schober, H. & Oligschleger, C. Low-frequency vibrations in a model glass. *Phys. Rev. B* **53**, 11469, DOI: [10.1103/PhysRevB.53.11469](https://doi.org/10.1103/PhysRevB.53.11469) (1996).
15. Mahajan, S. & Ciamarra, M. P. Unifying description of the vibrational anomalies of amorphous materials. *Phys. Rev. Lett.* **127**, 215504, DOI: [10.1103/PhysRevLett.127.215504](https://doi.org/10.1103/PhysRevLett.127.215504) (2021).
16. Lerner, E. & Bouchbinder, E. Boson-peak vibrational modes in glasses feature hybridized phononic and quasilocalized excitations. *The J. Chem. Phys.* **158**, DOI: [10.1063/5.0147889](https://doi.org/10.1063/5.0147889) (2023).

17. Moriel, A., Lerner, E. & Bouchbinder, E. Boson peak in the vibrational spectra of glasses. *Phys. Rev. Res.* **6**, 023053, DOI: [10.1103/PhysRevResearch.6.023053](https://doi.org/10.1103/PhysRevResearch.6.023053) (2024).
18. Richard, D. *et al.* Universality of the nonphononic vibrational spectrum across different classes of computer glasses. *Phys. Rev. Lett.* **125**, 085502, DOI: [10.1103/PhysRevLett.125.085502](https://doi.org/10.1103/PhysRevLett.125.085502) (2020).
19. Lubchenko, V. & Wolynes, P. G. The origin of the boson peak and thermal conductivity plateau in low-temperature glasses. *Proc. Natl. Acad. Sci.* **100**, 1515–1518, DOI: [10.1073/pnas.252786999](https://doi.org/10.1073/pnas.252786999) (2003).
20. Parisi, G. On the origin of the boson peak. *J. Physics: Condens. Matter* **15**, S765, DOI: [10.1088/0953-8984/15/11/302](https://doi.org/10.1088/0953-8984/15/11/302) (2003).
21. Taraskin, S. N., Loh, Y. L., Natarajan, G. & Elliott, S. R. Origin of the boson peak in systems with lattice disorder. *Phys. Rev. Lett.* **86**, 1255–1258, DOI: [10.1103/PhysRevLett.86.1255](https://doi.org/10.1103/PhysRevLett.86.1255) (2001).
22. Chumakov, A. I. *et al.* Equivalence of the boson peak in glasses to the transverse acoustic van hove singularity in crystals. *Phys. Rev. Lett.* **106**, 225501, DOI: [10.1103/PhysRevLett.106.225501](https://doi.org/10.1103/PhysRevLett.106.225501) (2011).
23. Baggioli, M. & Zaccone, A. Universal origin of boson peak vibrational anomalies in ordered crystals and in amorphous materials. *Phys. Rev. Lett.* **122**, 145501, DOI: [10.1103/PhysRevLett.122.145501](https://doi.org/10.1103/PhysRevLett.122.145501) (2019).
24. Marruzzo, A., Schirmacher, W., Fratallocchi, A. & Ruocco, G. Heterogeneous shear elasticity of glasses: the origin of the boson peak. *Sci. Reports* **3**, 1407, DOI: [10.1038/srep01407](https://doi.org/10.1038/srep01407) (2013).
25. Hu, Y.-C. & Tanaka, H. Origin of the boson peak in amorphous solids. *Nat. Phys.* **18**, 669–677, DOI: [10.1038/s41567-022-01628-6](https://doi.org/10.1038/s41567-022-01628-6) (2022).
26. Hu, Y.-C. & Tanaka, H. Universality of stringlet excitations as the origin of the boson peak of glasses with isotropic interactions. *Phys. Rev. Res.* **5**, 023055, DOI: [10.1103/PhysRevResearch.5.023055](https://doi.org/10.1103/PhysRevResearch.5.023055) (2023).
27. Jiang, C., Baggioli, M. & Douglas, J. F. Stringlet excitation model of the boson peak. *The J. Chem. Phys.* **160**, 214505, DOI: [10.1063/5.0210057](https://doi.org/10.1063/5.0210057) (2024).
28. Cunyuan, J. & Baggioli, M. Phonons in stringlet-land and the boson peak. *J. Physics: Condens. Matter* DOI: [10.1088/1361-648X/ad789c](https://doi.org/10.1088/1361-648X/ad789c) (2024).
29. Tømterud, M. *et al.* Observation of the boson peak in a two-dimensional material. *Nat. Phys.* **19**, 1910–1915, DOI: [10.1038/s41567-023-02177-2](https://doi.org/10.1038/s41567-023-02177-2) (2023).
30. Zhang, J., Zhang, H. & Douglas, J. F. A closer examination of the nature of atomic motion in the interfacial region of crystals upon approaching melting. *The J. Chem. Phys.* **160**, 114506, DOI: [10.1063/5.0197386](https://doi.org/10.1063/5.0197386) (2024).
31. Dauchot, O., Karmakar, S., Procaccia, I. & Zylberg, J. Athermal brittle-to-ductile transition in amorphous solids. *Phys. Rev. E* **84**, 046105, DOI: [10.1103/PhysRevE.84.046105](https://doi.org/10.1103/PhysRevE.84.046105) (2011).
32. Chattoraj, J. & Ciamarra, M. P. Role of attractive forces in the relaxation dynamics of supercooled liquids. *Phys. Rev. Lett.* **124**, 028001, DOI: [10.1103/PhysRevLett.124.028001](https://doi.org/10.1103/PhysRevLett.124.028001) (2020).
33. González-López, K., Shivam, M., Zheng, Y., Ciamarra, M. P. & Lerner, E. Mechanical disorder of sticky-sphere glasses. I. Effect of attractive interactions. *Phys. Rev. E* **103**, 022605, DOI: [10.1103/PhysRevE.103.022605](https://doi.org/10.1103/PhysRevE.103.022605) (2021).
34. González-López, K., Shivam, M., Zheng, Y., Ciamarra, M. P. & Lerner, E. Mechanical disorder of sticky-sphere glasses. II. Thermomechanical inannealability. *Phys. Rev. E* **103**, 022606, DOI: [10.1103/PhysRevE.103.022606](https://doi.org/10.1103/PhysRevE.103.022606) (2021).
35. Zheng, Y., Mahajan, S., Chattoraj, J. & Pica Ciamarra, M. Designing Phononic Band Gaps With Sticky Potentials. *Front. Phys.* **9**, 665391, DOI: [10.3389/fphy.2021.665391](https://doi.org/10.3389/fphy.2021.665391) (2021).
36. Falk, M. L. & Langer, J. S. Dynamics of viscoplastic deformation in amorphous solids. *Phys. Rev. E* **57**, 7192, DOI: [10.1103/PhysRevE.57.7192](https://doi.org/10.1103/PhysRevE.57.7192) (1998).
37. Vivek, S., Kelleher, C. P., Chaikin, P. M. & Weeks, E. R. Long-wavelength fluctuations and the glass transition in two dimensions and three dimensions. *Proc. Natl. Acad. Sci.* **114**, 1850–1855, DOI: [10.1073/pnas.1607226113](https://doi.org/10.1073/pnas.1607226113) (2017).
38. Illing, B. *et al.* Mermin–wagner fluctuations in 2d amorphous solids. *Proc. Natl. Acad. Sci.* **114**, 1856–1861, DOI: [10.1073/pnas.1612964114](https://doi.org/10.1073/pnas.1612964114) (2017).
39. Li, Y.-W. *et al.* Long-wavelength fluctuations and anomalous dynamics in 2-dimensional liquids. *Proc. Natl. Acad. Sci.* **116**, 22977–22982, DOI: [10.1073/PNAS.1909319116](https://doi.org/10.1073/PNAS.1909319116) (2019).
40. Zhang, H., Wang, X., Yu, H.-B. & Douglas, J. F. Fast dynamics in a model metallic glass-forming material. *The J. Chem. Phys.* **154**, 084505, DOI: [10.1063/5.0039162](https://doi.org/10.1063/5.0039162) (2021).

41. Pazmiño Betancourt, B. A., Douglas, J. F. & Starr, F. W. String model for the dynamics of glass-forming liquids. *The J. Chem. Phys.* **140**, 204509, DOI: [10.1063/1.4878502](https://doi.org/10.1063/1.4878502) (2014).
42. Shintani, H. & Tanaka, H. Universal link between the boson peak and transverse phonons in glass. *Nat. Mater.* **7**, 870–877, DOI: [10.1038/nmat2293](https://doi.org/10.1038/nmat2293) (2008).
43. Moshe, M., Sharon, E. & Kupferman, R. Elastic interactions between two-dimensional geometric defects. *Phys. Rev. E* **92**, 062403, DOI: [10.1103/PhysRevE.92.062403](https://doi.org/10.1103/PhysRevE.92.062403) (2015).
44. Mondal, C., Moshe, M., Procaccia, I. & Roy, S. Dipole screening in pure shear strain protocols of amorphous solids. *Phys. Rev. E* **108**, L042901, DOI: [10.1103/PhysRevE.108.L042901](https://doi.org/10.1103/PhysRevE.108.L042901) (2023).
45. Schirmacher, W. & Ruocco, G. *Heterogeneous Elasticity: The Tale of the Boson Peak*, chap. Chapter 9, 331–373.
46. Lemaître, A. *et al.* Anomalous elasticity and plastic screening in amorphous solids. *Phys. Rev. E* **104**, 024904, DOI: [10.1103/PhysRevE.104.024904](https://doi.org/10.1103/PhysRevE.104.024904) (2021).
47. Wu, Z. W., Chen, Y., Wang, W.-H., Kob, W. & Xu, L. Topology of vibrational modes predicts plastic events in glasses. *Nat. Commun.* **14**, 2955, DOI: [10.1038/s41467-023-38547-w](https://doi.org/10.1038/s41467-023-38547-w) (2023).
48. Baggioli, M. Topological defects reveal the plasticity of glasses. *Nat. Commun.* **14**, 2956, DOI: [10.1038/s41467-023-38549-8](https://doi.org/10.1038/s41467-023-38549-8) (2023).

Supplementary information

Density of vibrational modes

We compare the density of vibrational modes obtained from Fourier transforming the velocity autocorrelation function (points) and via the direct diagonalisation of the Hessian matrix in Fig. 7 for systems with 256k particles. In the figure, we also illustrate the Debye's prediction, $D_{\text{Debye}} = A_D \omega^{D-1}$. In 2D, $A_D = \frac{2}{8\pi\rho/(c_l^{-2}+c_s^{-2})}$, with ρ the number density and $c_l = \sqrt{\frac{K+\mu}{\rho}}$ and $c_s = \sqrt{\frac{\mu}{\rho}}$ the longitudinal and the transverse shear velocities. In 3D, $A_D = \frac{3}{18\pi^2\rho/(c_l^{-3}+2c_s^{-3})}$, $c_l = \sqrt{\frac{K+\frac{4\mu}{3}}{\rho}}$ and $c_s = \sqrt{\frac{\mu}{\rho}}$. We determine the bulk K and shear μ moduli by investigating the stress-strain relationships in the linear response regime.

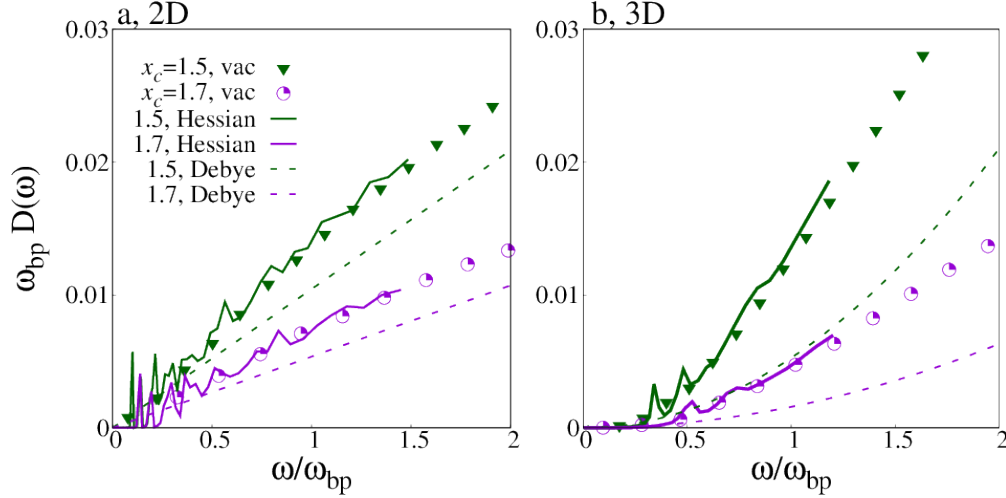


Figure 7. Different approaches to evaluate the vDOS. We compare diverse approaches to evaluating the vDOS, in 2D and 3D. Evaluating the vDOS by Fourier transforming the velocity autocorrelation function and via the diagonalization of the Hessian gives consistent results. Due to our system's large size, 256k particles, we compute only the lower end of the spectrum via the direct diagonalization of the Hessian.

Cage-relative measures filter plane waves at the boson peak

To evaluate the cage-relative ability to filter extended modes of norm $|\mathbf{u}|^2 = 1$, we consider $|\mathbf{u}^{\text{cr}}|^2$. Filtering occurs if $|\mathbf{u}^{\text{cr}}|^2 \ll 1$. As extended modes, we consider phonons with various wavelengths. There is no need to consider the superposition of phonons as the cage-relative 'operator' is linear, $(a\mathbf{u} + b\mathbf{v})^{\text{cr}} = a\mathbf{u}^{\text{cr}} + b\mathbf{v}^{\text{cr}}$. Any linear combination of 'filtered' displacement fields is also filtered.

Fig. 8 illustrates $|\mathbf{p}^{\text{cr}}|^2$ for phonon \mathbf{p} of wavelength λ , in two dimensions. The larger the phonon wavelength, the more efficient the filtering. Importantly, filtering is highly efficient at the wavelength $\lambda_{\text{bp}} = \frac{2\pi c_s}{\omega_{\text{bp}}}$ of the phonons expected to hybridize at the boson peak, as $|\mathbf{p}^{\text{cr}}|^2$ is in the range 10^{-4} to 10^{-3} , its value depending on the cutoff x_c of the interaction potential.

Density of vibrational defects

We define defects as clusters of particles whose cage-relative displacement is within the top $c = 5\%$. We explore how the density of defects, ρ_d , depends on the percentage c of particles with the highest cage-relative displacement.

As $c \rightarrow 0$, ρ_d vanishes since there are no clusters, meaning no particles meet the clustering criteria. As c increases, ρ_d grows, reflecting both the increasing size and number of clusters. However, beyond a certain point, as clusters begin to merge, ρ_d decreases, leading to a maximum in defect density at an intermediate c value.

Fig. 6a shows that, in 2D, the density of defects remains x_c independent for $c < 10\%$. Unless this threshold is considered unrealistically high, the exact value of c does not significantly affect our conclusions.

In 3D, the behavior of ρ_d for small x_c values is illustrated in Fig. 6c: ρ_d remains unchanged between $x_c = 1.8$ and $x_c = 1.7$ and increases as x_c decreases further. Thus, our results are not highly sensitive to the exact choice of x_c .

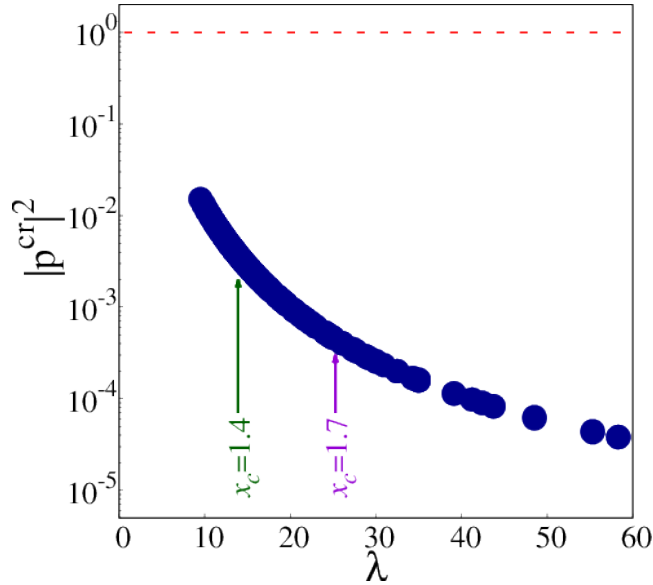


Figure 8. Filtering phonons via the cage-relative measured. Squared norm of the cage-relative displacement field $|\mathbf{p}^{\text{cr}}|^2$ associated with phonons ($|\mathbf{p}|^2 = 1$) of wavelength λ , in two dimensions. The vertical lines mark the wavelength λ_{bp} of phonons at the boson peak frequency for the extremal investigated x_c values. Analogous results hold in 3D.

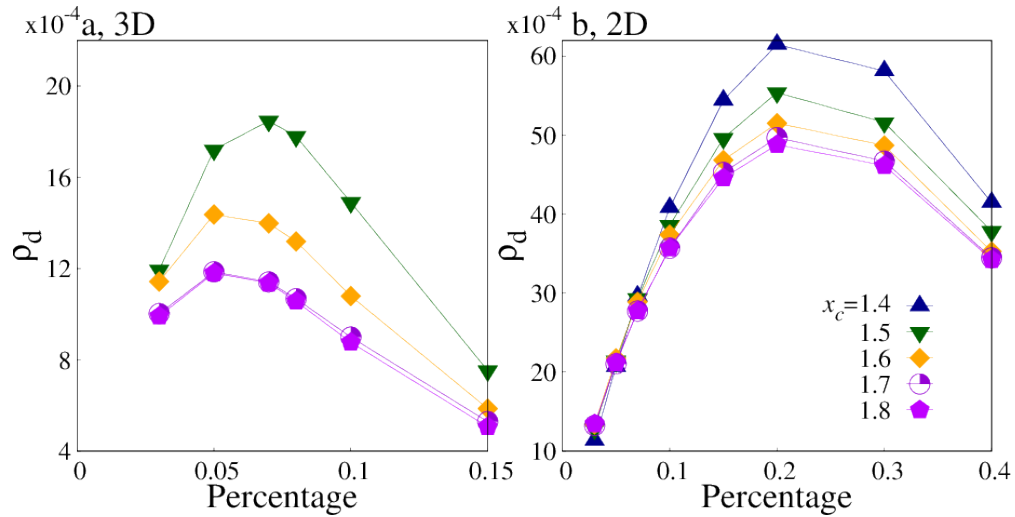


Figure 9. Cutoff dependence of the density of defects. We perform a cluster analysis of the $c\%$ of the particles with the largest magnitude of the cage relative displacement (in the mode at boson peak frequency) to identify the defects. **a** the density of defects ρ_d as a maximum as a function of c , and is roughly constant as c varies from 5% to 7%. **b** ρ_d remains constant in this c range for all x_c , also when we consider as defects only cluster with at least n_{min} particles. We illustrate the considered values of n_{min} for $x_c = 1.5$.